Spatial-Related Traffic Sign Inspection for Inventory Purposes Using Mobile Laser Scanning Data

Chenglu Wen, *Member, IEEE*, Jonathan Li, *Senior Member, IEEE*, Huan Luo, Yongtao Yu, Zhipeng Cai, Hanyun Wang, *Member, IEEE*, and Cheng Wang, *Member, IEEE*

***Abstract*—This paper presents a spatial-related traffic sign inspection process for sign type, position, and placement using mobile laser scanning (MLS) data acquired by a RIEGL VMX-450 system and presents its potential for traffic sign inventory applications. First, the paper describes an algorithm for traffic sign detection in complicated road scenes based on the retroreflectivity properties of traffic signs in MLS point clouds. Then, a point cloud-to-image registration process is proposed to project the traffic sign point clouds onto a 2-D image plane. Third, based on the extracted traffic sign points, we propose a traffic sign position and placement inspection process by creating geospatial relations between the traffic signs and road environment. For further inventory applications, we acquire several spatial-related inventory measurements. Finally, a traffic sign recognition process is conducted to assign sign type. With the acquired sign type, position, and placement data, a spatial-associated sign network is built. Experimental results indicate satisfactory performance of the proposed detection, recognition, position, and placement inspection algorithms. The experimental results also prove the potential of MLS data for automatic traffic sign inventory applications.**

***Index Terms*—Mobile laser scanning, traffic sign, detection, recognition, road surfaces, inventory and inspection.**

I. Introduction

TRAFFIC signs are a fundamental and essential element in road transportation systems because, in addition to their importance for traffic safety, they provide instructions to drivers and other road users. Traffic sign design specifications differ from country to country. However, the categories, graphic standards, and placement of traffic signs are all legally defined as standard [1], [2]. Nowadays, the continual expansion of cities creates an increasing demand for the installation of new signs and maintenance of existing signs based on inventory and inspection. Currently, traffic sign inventory procedures are mainly implemented manually or semi-automatically. These procedures require much time and labor to update the data, which makes it difficult to proceed on a regular basis. An efficient traffic sign inventory process is needed to accurately record sign data, such as the number of signs, type, condition and geographic location of each sign, as well as the spatial relations between the signs [3].

Traffic sign detection and recognition have been used for traffic sign automatic inventory in recent years [4], [5]. By detecting and recognizing the information from traffic signs and panels, sign detection and recognition mainly deals with information extraction and understanding tasks for further applications, such as traffic infrastructure surveys, intelligent driving aided systems, etc. [6]–[9]. Current sign detection and recognition research is based mainly on sign images and videos. Traffic signs exhibit ordinary shapes and standard colors; however, the extensive outlook variability of traffic signs is captured in uncontrolled situations, such as occlusion, drastic weather and illumination conditions, and image distortion and physical variation of the target surface. All these variations lead to tough working circumstances for image/video-based methods. Moreover, the output of the current traffic sign detection and recognition research mainly focuses on sign type [10], [11], or the geometric distribution (position) of traffic signs. However, spatial-related data is overlooked.

Sign placement, an important indicator for traffic sign condition evaluation, is relevant to the usability and visibility of traffic signs, and finally affects the road safety of the road users. The visibility status, such as the placement and appearance of the traffic signs, requires special concerns. Fig. 1 shows some examples of traffic signs that display a bad appearance or are poorly positioned. Periodic, automatic road surveying for spatial-related traffic sign inspection must be established to document, not only the traditional traffic sign inventory data, but also the spatial relations of the road environment associated with traffic signs (e.g., road surfaces, road markings, and vegetation). The surveyed data can be used to (1) maintain and reconstruct current sign resources and road infrastructure and (2) support the study of how traffic sign practices (e.g., appearance, position and placement) affect road safety.

As a type of Mobile Mapping System (MMS), the Mobile Laser Scanning (MLS) system collects geospatial data

Manuscript received October 8, 2014; revised February 12, 2015; accepted March 26, 2015. Date of publication April 20, 2015; date of current version December 24, 2015. This work was supported in part by the National Natural Science Foundation of China under Grants 61401382, 61371144, and 41471379. The Associate Editor for this paper was J. Zhang. *(Corresponding author: Cheng Wang.)*

C. Wen, H. Luo, Y. Yu, Z. Cai, and C. Wang are with Fujian Key Laboratory of Sensing and Computing for Smart City, School of Information Science and Engineering, Xiamen University, Xiamen 361005, China (e-mail: clwen@xmu.edu.cn; scholar.luo@gmail.com; allennessy.yu@gmail.com; azptc2h@gmail.com; cwang@xmu.edu.cn).

J. Li is with the MoE Key Laboratory of Underwater Acoustic Communication and Marine Information Technology, School of Information Science and Engineering, Xiamen University, Xiamen 361005 China, and also with the Department of Geography and Environmental Management, Faculty of Environment, University of Waterloo, Waterloo, ON N2L 3G1, Canada (e-mail: junli@xmu.edu.cn).

H. Wang is with the School of Electronic Science and Engineering, National University of Defense Technology, Changsha 410073, China (e-mail: why860314@126.com).

Color versions of one or more of the figures in this paper are available online at http://ieeexplore.ieee.org.

Digital Object Identifier 10.1109/TITS.2015.2418214

Fig. 1. Examples of traffic signs with bad placement or appearance (collected from Internet).

using calibrated multi-sensors (e.g., Global Navigation Satellite System/Initial Measurement Unit (GNSS/IMU) integration system, laser scanners, and high-resolution cameras) mounted on a mobile platform [12]. The MLS systems record the time-of-flight and the reflected energy of the laser beams from a surface and form the 3-D point clouds with high resolution of geometry and intensity information. With the acquisition of highly accurate and dense data, there is a great potential to apply the MLS systems to traffic sign inventory, especially in regard to the geospatial information achieved for creating the road environment spatial relations associated with traffic signs.

In this paper, we propose a spatial-related traffic sign inspection process based on vehicle-borne MLS data and specifically introduce its application to automatic traffic sign inventory. The flowchart of the proposed process is shown in Fig. 2. First, to extract the sign area from the road scene, a traffic sign detection process is proposed for the MLS point clouds. Secondly, a registration process is conducted to project the colored point clouds of the extracted sign area onto a defined 2-D image plane for further sign recognition. Then, with the advantages of the acquired accurate geo-referenced MLS data, the traffic sign position and placement inspection process is conducted by modeling the spatial relationship among the traffic sign and road elements. Finally, sign type is assigned by a support vector machine (SVM) classifier trained by a mix feature of Histogram of Gradients (HOG) and color descriptor. With the above position and placement data, a spatial-associated sign network is built for a certain sign type.

The rest of the paper is organized as follows. A review of the previous work is given in Section II. The MLS system and the collected data sets are described presented in Section III. The traffic sign detection process is presented in Section IV. The algorithm for traffic sign position and placement inspection are detailed in Section V. The sign type recognition for spatial-associated sign network building is described in Section VI. Experimental results and conclusions are presented in Sections VII and VIII, respectively.

II. Related Work

A. Studies on Traffic Sign Detection and Recognition

As an essential component of the intelligent transportation system, traffic sign recognition (TSR) has developed rapidly in recent years. The TSR methods generally consist of sign detection and sign recognition. Most of the current TSR-related works remain focused on developing robust feature extractors and descriptors, or recognition models. Several public data sets [13], [14] have been used to assess the pros and cons of TSR. Because the data update in these data sets is time consuming and labor intensive, these data sets are appropriate for TSR research, but inappropriate for traffic sign status inspection.

Using color or shape information of the traffic sign and panel, much effort has been made to extract visual appearance features from the images and videos [15]. To achieve a reliable detection performance under different lighting situations, traffic sign detection works have been conducted based on Y'CBCR [16], HSV [17], and CIECAM97 [18] color models. Except for global features, local invariant features, such as points of interest/regions [19], MSER [20], and Hough-like feature [21], have also been used in traffic sign detection. Moreover, Gonzalez-Jorge *et al.* [22] applied a 3-D laser scanner for traffic sign detection and reflectance inspection regarding the highly reflective radiation on traffic signs.

Most of the existing traffic sign detection methods, based on color and shape information, have relatively strict data requirements. Detection performance highly depends on the environmental conditions, such as illumination, occlusion, viewpoint, and weather conditions. Also, shape-related local feature-based methods are usually time consuming and computationally intensive for such large volumes of data. In addition, for traffic sign detection tasks only, almost all the existing detection methods must be conducted in the daytime.

There are many published results related to TSR based on images [23], [24] or videos [25] using local features. Ruta *et al.* [26] proposed a sign recognition method based on similarity measurement learning from example pairs. Yuan *et al.* [27] developed color global and local oriented edge magnitude pattern features for traffic sign description and applied an SVM for recognition. Except for the feature detectors and descriptors, some machine learning algorithms such as random forest [28] and neural network [29], also have been utilized for sign recognition [30], [31].

B. Studies on Automatic Traffic Sign Inventory

The literature contains studies on the detection, recognition, and 3-D localization of traffic signs via multi-view images [32]. The precision of localization and spatial relations of a road scene are dependent on the reconstruction algorithm based on multi-view images. Recently, image/video and GPS-based methods have been applied to traffic sign inventory [33].

Image-based MMS has been applied to traffic-sign related survey and mapping tasks in recent years. Habib *et al.* [34] applied an MMS to traffic sign inventory and achieved traffic sign data, including sign type, height above the pavement, offset from road edge, coordinate location, and size of the sign. However, the image-based MMS survey requires conducted

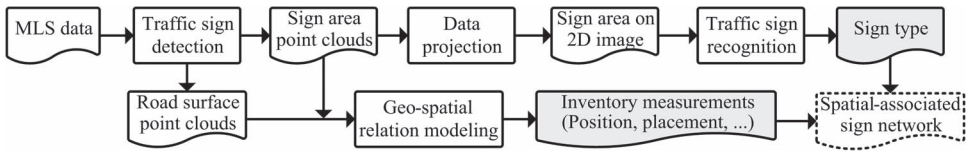

Fig. 2. Flowchart of the proposed method for traffic sign type recognition, position and placement inspection.

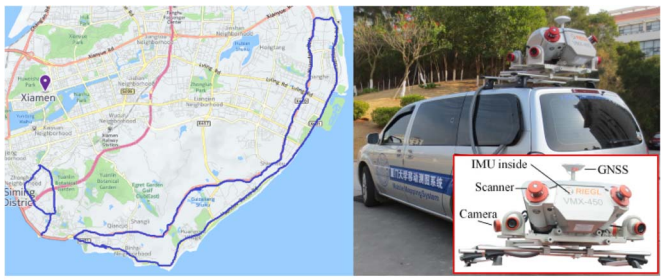

Fig. 3. Roads and system for MLS data acquisition: (a) trajectory (in blue color) in Xiamen Island for data acquisition, (b) MLS system used.

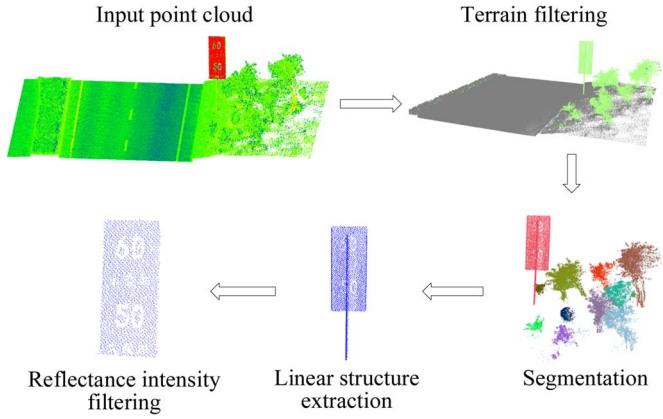

Fig. 4. Illustration of the proposed traffic sign detection in MLS point clouds.

under good lighting conditions. Also, the relationships between traffic signs and road environment, such as the angle between the sign plane and road surface, and the angle between the sign plane and lane driving direction, must be analyzed further.

Compared to photogrammetry and field surveys, an MLS system captures high point-density and accurate 3-D point clouds in a short time period [35]. MLS systems have been applied to transportation-related surveys [36], for example mapping and extraction curbstone [37] and road markings [38]. Pu *et al*. [39] recognized basic road traffic structures from mobile laser scanning data. Also, terrestrial and static laser scanning systems have been used in simple traffic sign inventory applications [22]. However, there is little research work related to systematic and automatic traffic sign inventory based on MLS systems.

III. MLS System and Data Acquisition

The traffic sign MLS data is acquired in the area within Xiamen Island (longitude 118° 04′ 04″ E, latitude 24° 26′ 46″ N), a part of the City of Xiamen (Fig. 3(a)). A RIEGL VMX-450 system, mounted on a minivan, is used to acquire the MLS data (Fig. 3(b)). This system is smoothly integrated with 1) two RIEGL VQ-450 laser scanners, 2) four high-resolution digital cameras, 3) a GNSS, 4) an IMU, and 5) a wheel-mounted distance measurement indicator (DMI). These two laser scanners are installed on both sides of the main frame with an "X" configuration pattern and rotate to emit laser beams. The maximum valid range of the laser beams are approximately 800 m. Two of the four RIEGL CS-6 high-resolution (2452 by 2056 pixels) color digital cameras are installed on the left side of the frame and the other two on the right side of the frame. More information about the MLS system's specifications can be found in [40].

Three surveys were performed with MLS to obtain the data required for this research. The Ring Road that is used for survey is a seaside green-corridor for tourism with a speed limit of 60–70 km/h and contains different kinds of traffic signs. The Ring Belt Road (including a tunnel) that is used for survey is a busier inner-city road, with a speed limit of 50–60 km/h. The Zhongshan Road that is used for survey is a much busier road, with a speed limit of 30–40 km/h, and contains many crossings and more dense traffic signs. The three roads have different speed limits, traffic flows, and traffic sign placements. These roads provide various MLS data of traffic signs according to different road situations. The Ring Road data set contains about 800 million points and has a road section of approximately 20 km. The Ring Belt Road data set contains about 400 million points and has a road section of approximately 10 km. The Zhongshan Road data set contains about 300 million points and has a road section of approximately 7 km. Samples of more than 260 MLS traffic sign scenes and 500 traffic sign images were collected for further testing.

IV. Traffic Sign Detection in MLS Data

In our automatic traffic sign inspection process, a sign detection algorithm is firstly used to detect the signs on both MLS point clouds and image data. In the detection stage, the traffic sign target is extracted from the MLS point cloud and projected onto the image region that embodies this traffic sign. Here, the traffic sign surface is defined as a highly retro-reflective vertical plane in the MLS data that can be used for traffic sign detection and extraction.

A. Traffic Sign Detection Based on MLS Point Clouds

The proposed algorithm for detecting traffic signs is based on both the linear structure of the traffic sign pole and the retro-reflectance of the sign surface in the MLS point clouds. The detection procedure is divided into three main steps: terrain points filtering, linear structured objects detecting, and reflectance intensity based sign surface filtering. Fig. 4 shows an illustration of the proposed detection process.

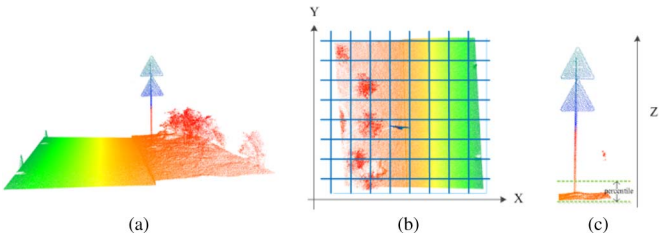

Fig. 5. Grid representation of MLS point clouds: (a) a point clouds scene, (b) XY horizontal plane, (c) cell point selection.

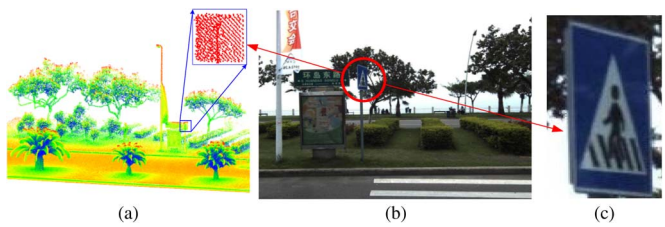

Fig. 6. Illustration of projecting the traffic sign point clouds onto a 2-D image: (a) MLS point clouds and sign area detected, (b) image acquired along with the MLS data, (c) traffic sign area projected onto a 2-D image.

A terrain filter is firstly used to separate off-terrain points (e.g., vegetation, small objects, moving objects such as vehicles, etc.) from terrain points. The filtering process is based on a grid representation of the data at each level. For a MLS point clouds scene (Fig. 5(a)), the first step is to specify a coarse grid in the XY-plane, which is defined as the horizontal plane (Fig. 5(b)). For each non-empty cell of the grid, we select a point according to the given percentile which specifies the percentage of points within a cell that shall be below the representative cell point (Fig. 5(c)). Then, each representative cell point, together with its neighboring cells' representative points, is used to estimate a local plane. After that, for each cell, a bounding box with a certain distance range above/below its estimated plane is defined. Those points, which are outside the tolerance range, are marked as "off-terrain" points and not considered further. The remaining points are assigned to one of the four sub-cells of the next finer level, and again the representative cell points are determined. The process is repeated until the finest level is reached. Then, a Euclidean clustering algorithm is applied to segment the off-terrain points into clusters. Following [41], the maximal eigenvalue (λ_1), the second and the minimal eigenvalues (λ_2 and λ_3) of the local covariance matrix of a linear structure satisfy the following condition: $\lambda_1 \gg \lambda_2 \approx \lambda_3$, and $\lambda_1/\lambda_2 > 10$. Based on this criterion, the points in each cluster are classified as linear and nonlinear structures. The clusters that contain the number of linear structural points less than a given threshold (setting as 50) are removed.

The retro-reflectance properties of the traffic sign front surfaces generally have a strong reflectance intensity in MLS point clouds. As the final step for the proposed sign detection algorithm, we extract the traffic sign surfaces according to the reflectance intensity and remove the points with intensities below 60 000. This step works especially well under bad weather conditions, such as fog, low/strong illumination, and detection tasks at night. Meanwhile, the existing image/video-based traffic sign detection algorithms have difficulty working under such conditions.

B. On-Image Sign Detection by Point Clouds Projection

Based on the detected sign point clouds, on-image sign area detection is implemented by projecting the 3-D points of each traffic sign onto a 2-D image to provide appearance information for further sign type recognition. The on-image sign area detection process includes the following two steps: 1) map the 3-D points in the world coordinate system onto the camera coordinate system, 2) project the points in the camera coordinate system onto the image plane defined by the camera system in VMX-450.

Denote CMCS as the camera coordinate system, BODY as the vehicle coordinate system, ECEF as the global coordinate system (WGS84 system used in our study), and NED as the north east down coordinate system. Mapping a 3-D point in MLS data in CMCS has three transformation steps as ECEF-to-NED, NED-to-BODY and BODY-to-CMCS. The VMX-450 system provides three transformation matrices ($C_{ECEF2NED}, C_{NED2BODY}$, and $C_{BODY2CMCS}$) for these transformation steps, respectively. A 3-D point P_{ECEF} acquired by VMX-450 system in ECEF is transformed into the point, P_{CMCS}, in camera coordinate system CMCS by applying the following:

$$P_{CMCS} = C_{BODY2CMCS} * C_{NED2BODY} * C_{ECEF2NED} * P_{ECEF}. \quad (1)$$

Then, the point P_{CMCS} is projected onto a 2-D image plane by obtaining the correspondent image pixel coordinates according to the 3-D points in the CMCS system. Regarding the original image's radial distortion acquired by the MLS system, a camera calibration model is applied to obtain distorted image coordinates [42]. As for tolerating registration error between the MLS point clouds and images, we enlarged the sign area in images with threshold ρ (setting as 10).

An example of the on-image sign detection is shown in Fig. 6. In this example, an image of a scene is acquired with relatively low illumination, far acquiring distance, and large viewpoint. Under these conditions, the image-based detection methods have difficulty performing; whereas the proposed method is able to correctly detect the traffic sign in the image.

V. Traffic Sign Position and Placement Inspection

The accurate geo-spatial relations built for the traffic signs and the associated road elements is the unique characteristic of the proposed traffic sign inspection process based on MLS data. Here, we present the automatic inspection of position and placement of traffic signs as examples. With the MLS data, the position of every point of the traffic sign and associated road surface is accurate within millimeters. Sufficient measurements can be further acquired according to specific requirements.

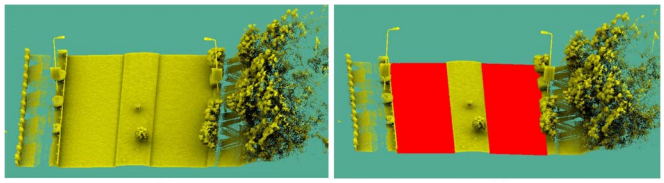

(a) (b)

Fig. 7. Illustration of road surface extraction: (a) original point cloud, (b) road surface extracted (shown in red color).

A. Road Surface and Boundary Extraction

Before evaluating the aforementioned position and placement parameters, the road boundaries in MLS point clouds are firstly located. In our previous work [40], we developed a curb-based method for extracting road surface points from MLS point clouds. First, by using the vehicle's trajectory data, which are recorded by the onboard navigation systems, a raw point cloud is vertically partitioned into a set of data segments with a length of approximately 3 m perpendicularly to the direction of travel. Then, each data segment is sampled to generate a vertical profile perpendicularly to the trajectory. Next, the generated profiles are further gridded to ascertain principal points from each of the grids by using a layering approach. The ascertained principal points within each profile form a pseudo scan line for the detection of curb points. Afterwards, curb points are determined by ascertaining the first two principal points located on opposite sides of the trajectory with specific elevation gradient constraints. Finally, the extracted curb points from all profiles are fitted to form curb-lines, which represent the boundaries of the road and are used to separate road surface and roadside points.

In this paper, we use this curb-based method [40] to extract road boundaries and separate the road surface points from roadside points in the point clouds. In Section IV-A, ground points are segmented from the entire point cloud. Since the segmented ground points contain both road surface points and roadside points, the segmented ground points are used to extract road boundaries and segment road surface points from roadside ground points. An example of the road surface extraction is shown in Fig. 7.

B. Traffic Sign Positioning Parameter Measurement

The position and type of traffic sign information can be embedded into many intelligent transportation related applications. In this paper, we define a traffic sign's position as the coordinates of the centroid of the bottom ring of the traffic sign pole. By such a definition, the position, instead of a real point on the traffic sign, is actually a floating point at the bottom of a traffic sign.

To compute the position of a traffic sign using MLS point clouds, first, the point, p, with the lowest elevation (denoted as h_p) on the traffic sign pole is determined (Fig. 8(a)). Then, a horizontal profile with a thickness size, s_t (2 cm used), is generated by including the points with elevations within the range h_p to $h_p + s_t$ on the traffic sign pole. Next, a horizontal circle C is fitted from the points within the horizontal profile (Fig. 8(b)). Finally, the x and y coordinates of the traffic sign

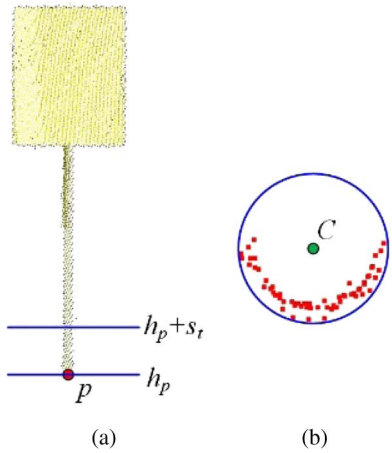

Fig. 8. Illustration of traffic sign position calculation: (a) lowest-elevation point selection and horizontal profile generation, (b) horizontal profile fitting and circle center determination.

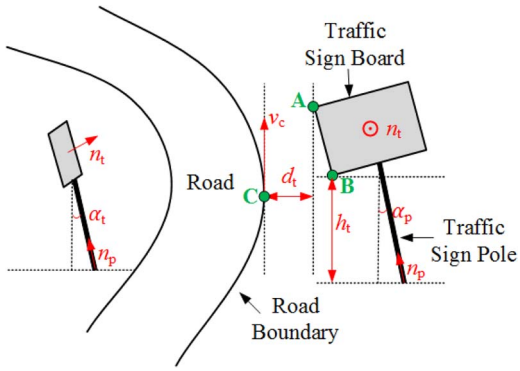

Fig. 9. Illustration of traffic sign placement calculation.

position are assigned, respectively, to the x and y coordinates of the center of the fitted circle C, and the z coordinate is assigned to the z coordinate of point p.

C. Traffic Sign Placement Parameters Measurement

In this paper, the following parameters are measured for evaluating traffic sign placement : 1) height of the traffic sign above the ground (h_t), 2) distance of the traffic sign from the road boundary (d_t), 3) orientation of the traffic sign with respect to the road direction (α_d), 4) inclination of the traffic sign with respect to the traffic sign board orientation (α_t), 5) inclination of the traffic sign with respect to the traffic sign board profile (α_p), and 6) planarity of the traffic sign.

As shown in Fig. 9, h_t is defined as the height of the lowest point on the traffic sign board (point B) over the ground. The horizontal distance, d_t, between the point with the shortest horizontal distance to the road on the traffic sign board (point A) and the road boundary point closest to the traffic sign in the horizontal plane (point C) is defined as:

$$d_t = \sqrt{(x_A - x_C)^2 + (y_A - y_C)^2} \tag{2}$$

where x_A and x_c are the x coordinates of points A and C, respectively, and v_A and v_c are the y coordinates of points A and C, respectively. The horizontal angle, α_d, included between

the tangent vector of point C (v_c) and the normal vector of the traffic sign board (n_t) is defined as:

$$a_d = \arccos\left(v_c^x n_t^x + v_c^y n_t^y\right) \tag{3}$$

where v_c^x and n_t^x are the x components of v_c and n_t, respectively, and v_c^y and n_t^y are the y components of v_c and n_t, respectively. The angle included, α_t, between the traffic sign pole's distribution direction (n_p) and the vertical direction with respect to the traffic sign board's orientation is defined as:

$$a_t = \arcsin\left(n_t^z\right) \tag{4}$$

where n_t^z is the z component of n_t. The angle included, α_p, between the traffic sign pole's distribution direction (n_p) and the vertical direction with respect to the traffic sign board's profile is defined as:

$$a_p = \arcsin\left(n_p^z\right) \tag{5}$$

where n_p^z is the z component of n_p; the traffic sign's planarity is measured by the standard deviation of the laser points on the traffic sign board.

The fitted curb-lines and segmented roadside ground points are used to compute the above parameters. To measure h_t, the points on the traffic sign board are first projected onto a horizontal plane to calculate a horizontal bounding box for the traffic sign board. Then, the ground points within the bounding box are selected to fit a ground plane. Finally, h_t is assigned as the height of the lowest point, B, on the traffic sign board over the ground plane.

To measure d_t, first, the corner point A on the traffic sign board, whose vertical line segment dropped from this corner point has the shortest distance to the curb-line, is determined. For a round-shaped traffic sign, the bounding rectangle of the traffic sign board is used for the determination of point A. Then, the corresponding curb-line, point C, with the shortest distance to the traffic sign is selected. Finally, d_t is assigned as the horizontal distance between points A and C. To measure α_d, first, the points on the traffic sign board are used to construct a covariance matrix. After eigenvalue decomposition on the covariance matrix, the normal vector, n_t, of the traffic sign board is obtained. Then, the tangent vector, v_c of point C is calculated using the fitted curb-line. Finally, α_d is assigned as the horizontal angle included between vectors n_t and v_c.

To measure α_t, and α_p, first, the points on the traffic sign pole are used to construct a covariance matrix. After eigenvalue decomposition on the covariance matrix, the distribution direction, n_p, of the traffic sign pole is obtained. Then, α_t is assigned as the angle included between n_p and the vertical direction with respect to n_t. α_p is assigned as the angle included between n_p and the vertical direction with respect to the perpendicular direction of n_t. To measure the planarity of the traffic sign, first, the points on the traffic sign board are fitted to form a plane. Then, the planarity is assigned as the standard deviation of these points with respect to the fitted plane.

With above traffic sign placement parameters measured, the abnormality and usability of the traffic signs can be evaluated. For example, if the value of α_d is too large, the orientation of the traffic sign is bad for conducting traffic activities. If the value of α_t is too large, the traffic sign is not installed in an upright position. These parameters influence the usability of the traffic signs and can help to accurately evaluate sign conditions.

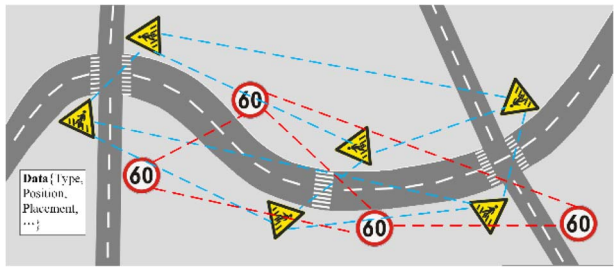

Fig. 10. Illustration of the spatial-associated traffic sign network.

VI. Sign Type Recognition for Spatial-Associated Sign Network Building

In automatic traffic sign inventory applications, sign type is usually given by a TSR process. The recognition stage labels bounding fields according to the enclosed traffic sign and resembles the sign type classification problem. In our method, the traffic sign type is obtained by an image-based TSR process using the detection results from the on-image sign detection by point clouds projection. Two types of features are used to represent the visual characteristics of a traffic sign. Following [43], a concatenation of hue histogram with the scale-invariant feature transform (SIFT) descriptor, the HueSIFT, is extracted as color descriptor. The HOG feature [44] is used as a local descriptor of a traffic sign. The SVM classifier is adapted as the recognition model. Since the TSR work is not the main focus of our study, we demonstrate only the sign type recognition process in our method. Also, there is much work about TSR that can be further applied to our traffic sign inspection process.

Besides giving the sign type, the uniqueness of our inspection process is that we give accurate spatial coordinates (position) and placement for each recognized traffic sign and also build accurate geo-spatial relations between the recognized traffic signs (same or different sign types). With the achieved position and placement information for a traffic sign, a spatial-associated network for traffic signs of the same type can be built (Fig. 10). The node of the network represents the recognized traffic sign; nodes with a certain type of attribute are associated in the network by position attributes.

VII. Experiments and Discussions

A. Traffic Sign Detection on MLS Point Clouds and Image Data

We tested the detection accuracy on the data sets selected from the survey conducted on June 2, 2014 (Ring Road and Ring Belt Road) and February 3, 2015 (Zhongshan Road). To test the detection algorithm on MLS data, 264 point cloud scenes were used. To test the detection algorithm on images, 327 image samples were used. Some examples of traffic signs detected by the proposed algorithm are shown in Fig. 11. The images are acquired while the MMS is driven on the road, the images possess varied viewpoints (some of which are large).

Fig. 11. Examples of traffic signs detected by the proposed detection algorithm.

TABLE I
THE QUANTITATIVE ASSESSMENT OF THE PROPOSED TRAFFIC SIGN DETECTION ALGORITHM

	Method in [45]	Detection on MLS data	Detection on 2D image
Total number	264	264	501
Correctly detected (TP) number	239	241	464
Partially detected number	0	16	Merge into FN
Missed (FN) number	25	16	37
False alarm (FP) number	21	22	36
Precision (%)	91.92	91.63	92.61
Recall (%)	90.53	93.77	92.80
F_1 Measure (%)	91.22	92.69	92.71

1) Quantitative Assessment of the Proposed Detection Algorithm: For quantitative assessment purposes, we compared the extracted traffic signs with the manually labeled reference data, as well as a detection method based on MLS point clouds presented in [45]. Similar to the evaluation criteria used in [26], TP ("correctly detected") represents the percentage of the correctly detected testing samples in the reference data. "Partially detected" represents the percentage of the testing samples that are partially detected. FN ("missed") represents the percentage of the undetected testing samples, and FP ("false alarm") represents the percentage of the falsely detected non-traffic signs. Precision, recall, and F_1 measure values are used to evaluate the accuracy of the detection algorithm as follows:

$$\text{Precision} = \frac{TP}{TP + FP} \tag{6}$$

$$\text{Recall} = \frac{TP}{TP + FN} \tag{7}$$

$$F_1 \text{ measure} = \frac{2 * TP}{2 * TP + FN + FP}. \tag{8}$$

All these three values were computed for the proposed detection algorithm on MLS data, the detection algorithm on 2-D images, and method in [45] (see Table I).

As seen in Table I, a precision value of 91.63% is obtained for the detection algorithm on MLS data. Out of 264 traffic signs, 241 are correctly detected using point cloud data. Sixteen samples are missed by the detection algorithm. The two reasons for the missed traffic signs are 1) the acquisition of incomplete point clouds and 2) the acquisition of non-reflective side signs. For example, point clouds of some traffic signs are acquired from the opposite direction of the lane, and the back sides of the traffic signs (without reflective material) are scanned. Our algorithm fails to detect these traffic signs. There are sixteen partially detected traffic signs, whose point clouds are heavily occluded by vegetation or other objects; thus, these traffic signs are impossible to detect by the image-based method. Twenty two samples, mostly advertising boards with similar linear structures and reflectance intensities, are detected as false positives. For the same data, method in [45] achieves a precision and recall of 91.92% and 90.53%, respectively. Twenty five traffic signs are missed caused by severe occlusions of trees. In addition, 21 false alarms are generated because of high similarities of other objects to the traffic signs in the scene. Compared to method in [45], our method achieves closed precision, and higher recall and F_1 measure values.

(a) (b) (c)

Fig. 12. Examples of traffic sign detected in challenging scenarios. (a) strong illumination and large viewpoint, (b) partial occlusions, (c) cluttered background.

For one MLS scene, several images were obtained with different viewpoints and distances while our RIEGL VMX-450 system (with 4 color digital cameras) was driven on the road to collect both the point clouds and image data. Out of 501 image samples, 464 are correctly detected when testing the proposed on-image detection algorithm. With the projection process, the precision rate reaches 92.61%. Because the point clouds acquired for a traffic sign are too sparse and the size of a traffic sign in an image is too small, the on-image detection algorithm misses 37 samples. Thirty six samples, detected as false positives, are mostly the false positives brought about by the previous detection results. Also, the calibration error between the laser scanners and cameras in MMS makes multi-targets coexist while projecting point clouds onto an image, and finally causes false positives.

2) Traffic Sign Detection in Challenging Scenarios: Fig. 12 shows some examples of the detection results related to the challenging scenarios of strong illumination and large viewpoint, partial occlusions, and cluttered background. The green blocks are the manually labeled detection results; the red blocks are our detection results.

Traffic sign surfaces are very distinctive, with high retro-reflectance intensity, in MLS data. Our detection process can be performed under adverse weather conditions, such as fog, rain, and strong illumination (Fig. 12(a)), as well as at night time. Unlike images, the MLS data contain full 3-D information, and there are no viewpoint and scale problems. Especially, because laser beams can travel through vegetation of certain densities, MLS data can detect traffic signs that are partially occluded by vegetation (Fig. 12(b)). For urban areas, traffic sign data are usually acquired with cluttered backgrounds, including vehicles, pedestrians, etc. Since a geo-spatial relation is used to separate traffic signs from other objects, our detection algorithm works well in cluttered backgrounds (Fig. 12(c)).

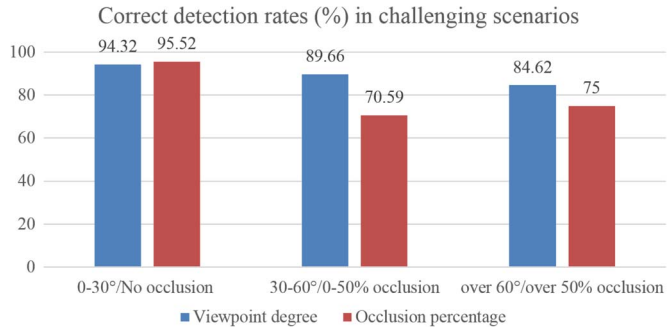

Fig. 13. Correct detection rates in challenging scenarios.

TABLE II
RECOGNITION RESULTS OF TRAFFIC SIGN TYPES

	HOG+HueSIFT+SVM	HoG+RandFor	HoG+HueSIFT+RandFor
Precision (%)	96.32	94.17	93.87

To quantitatively validate the performance of the proposed detection method in challenging scenarios, we present two histograms in Fig. 13 based on the detection results in Table I. The viewpoint degree histogram gives the detection correct rate according to different viewpoints of images. Here, we can calculate the viewpoint value for each image by the pose information of the MMS and the normal vector of the traffic sign board achieved in Section V-C. The occlusion percentage histogram gives the detection correct rate according to different occluded percentage of the signs. Here, we did not present the quantitative validation result for cluttered background since it is difficult to specify the degree of the background being cluttered. The results indicate that our detection method is capable of correctly detecting certain samples with large viewpoint and high percentage of occlusion (even over 60° viewpoint and over 50% occlusion).

B. Sign Type Recognition

To evaluate the sign type recognition performance, 2844 traffic sign images of eight classes, picked from data set [13], were used as training samples. 327 traffic sign images of eight classes, correspondently selected from the 501 sign images (total images in Table I), were used as testing samples. The 31 dimensions of HOG features were extracted. For HueSIFT color descriptor extracted, the lengths are 128 bins for SIFT, 1-D histogram of 37 bins, and 2-D descriptor of 121 bins in total. Two recognition models, SVM and Random Forest (RandFor) [46], were compared. The following three feature and model combinations were compared for sign type recognition: 1) HOG+HueSIFT+SVM, 2) HoG+RandFor, and 3) HoG+HueSIFT+RandFor. The experimental result is given by the precision value, i.e., from among the entire number of testing samples, the percentage of the samples that are correctly recognized.

As shown in Table II, a precision value of 96.32% is obtained for the proposed feature and model combination (HOG+HueSIFT+SVM) when testing our image data. A precision value of 94.17% is obtained for the HoG+RandFor combination, and a precision value of 93.87% is obtained for the HoG+HueSIFT+RandFor combination.

C. Traffic Sign Position Inspection Evaluation

To quantitatively evaluate the accuracy of the proposed algorithm in inspecting traffic sign positions, a Leica total station TS 15i-1 and a Leica RTK GS15 were used to collect on-site measurement data as the ground truth. It is difficult to measure the coordinates of the centroid of the traffic sign pole's bottom ring. Therefore, in practice, for computing the real position of each traffic sign, we measured the coordinates of three points, which were located 1) on the same horizontal plane, 2) around the bottom surface of the traffic sign pole, and 3) on the bottom surface of the traffic sign pole. Based on the three measured points, the Leica total station easily inferred the arc center of these three points. The coordinates of the inferred arc center were regarded as the ground truth for depicting the position of the traffic sign. In this paper, we selected a total number of 50 traffic signs of different shapes and statuses for evaluating the performance of the proposed algorithm. For illustration, 10 of the 50 typical traffic signs were selected. The measured ground truth data are listed in the left column of Table III. Correspondingly, the position information was also computed by our proposed algorithm using the MLS point cloud data. The experimental results for traffic sign positions (all in the WGS 84 coordinate system) are detailed in the middle column of Table III.

To assess the accuracy of the experimental results with respect to the ground truth, the biases between the two groups of coordinates were analyzed, as shown in the right column of Table III. Our proposed method achieved biases of ± 0.231 m, ± 0.287 m, and ± 0.442 m in the x, y, and z directions, respectively, on these 10 traffic signs. On a whole, our proposed method attained biases of ± 0.245 m, ± 0.292 m, and ± 0.449 m in the x, y, and z directions, respectively, on the 50 selected traffic signs. The proposed method obtained the best accuracy in the x direction; whereas the worst accuracy occurred in the z direction. The reason behind this phenomenon is that a part of the bottom of the traffic sign pole was cut off when removing the ground points, thereby resulting in great biases in the elevations. With the acquisition of spatial-related data, our proposed inspection method, using MLS point clouds, provides a promising means for inspecting traffic sign positions and achieves decimeter-level positioning accuracy. It can be noticed that no control point is used in the test, and the accuracy of the positioning parameter measured will be further improved when control points are considered during the data acquisition.

D. Traffic Sign Placement Inspection Evaluation

To quantitatively assess the accuracy of the proposed algorithm for measuring traffic sign placement parameters, we used a Leica total station TS 15i-1, which provides millimeter level measurements to collect on-site measurement data as the ground truth. A total of 50 traffic signs were measured by the total station unit and used as reference samples. Because it is

TABLE III
GROUND TRUTH AND POSITION MEASUREMENT RESULTS

Sample number	Ground Truth (WGS84)			Measurement (WGS84)			Bias		
	x (m)	*y* (m)	*z* (m)	*x* (m)	*y* (m)	*z* (m)	*x* (m)	*y* (m)	*z* (m)
1	-2737938.874	5124888.802	2621786.757	-2737938.716	5124889.089	2621787.152	0.158	0.287	0.395
2	-2737974.075	5124868.534	2621787.057	-2737973.844	5124868.780	2621787.412	0.231	0.246	0.355
3	-2738000.272	5124853.906	2621786.709	-2738000.167	5124854.156	2621787.069	0.105	0.250	0.360
4	-2738018.014	5124843.829	2621786.422	-2738017.952	5124843.607	2621786.706	-0.062	-0.222	0.284
5	-2738067.955	5124818.627	2621780.392	-2738067.942	5124818.435	2621780.834	0.013	-0.192	0.442
6	-2738154.099	5124786.009	2621751.616	-2738154.068	5124786.196	2621751.946	0.031	0.187	0.330
7	-2738125.006	5124783.995	2621786.228	-2738124.920	5124783.737	2621786.636	0.086	-0.258	0.408
8	-2738159.282	5124772.152	2621773.349	-2738159.233	5124772.292	2621773.738	0.049	0.140	0.389
9	-2738166.502	5124769.763	2621770.095	-2738166.381	5124769.648	2621770.441	0.121	-0.115	0.346
10	-2738221.891	5124755.369	2621741.177	-2738221.775	5124755.190	2621741.535	0.116	-0.179	0.358
Accuracy							±0.231	±0.287	±0.442

TABLE IV
GROUND TRUTH AND PLACEMENT PARAMETER COMPUTING RESULTS AND ACCURACIES

Sample number	h_t (m)			d_t (m)			α_t (degrees-minutes-seconds)			α_p (degrees-minutes-seconds)		
	Ground Truth	Result	Error	Ground Truth	Result	Error	Ground Truth	Result	Error	Ground Truth	Result	Error
1	5.51	5.54	0.03	-4.36	-4.43	-0.07	23”	1’11”	49”	1’43”	2’09”	26”
2	5.39	5.33	-0.06	-3.32	-3.28	0.04	1’15”	1’33”	18”	48”	1’21”	33”
3	5.12	5.16	0.04	-2.56	-2.59	-0.03	20”	1’05”	45”	25”	1’02”	37”
4	2.02	2.03	0.01	1.49	1.54	0.05	46”	1’38”	52”	2’17”	1’48”	-29”
5	5.33	5.30	-0.03	-3.33	-3.30	0.03	1’33”	2’19”	46”	1’38”	1’11”	-27”
6	2.21	2.25	0.04	1.47	1.52	0.05	1’21”	2’02”	41”	3’05”	2’50”	-15”
7	5.47	5.44	-0.03	-4.39	-4.33	0.06	37”	1’25”	48”	56”	1’23”	27”
8	5.44	5.40	-0.04	-3.33	-3.36	-0.03	2’19”	2’05”	-14”	2’46”	2’21”	-25”
9	2.17	2.12	-0.05	1.52	1.46	-0.06	1’02”	1’41”	39”	1’58”	2’19”	21”
10	5.32	5.28	-0.04	-3.35	-3.29	0.06	55”	1’39”	44”	1’04”	1’32”	28”
Accuracy		±0.063			±0.076			±52”			±37”	

very difficult to measure orientation angles, (α_d), in practice, we collected only 1) the ground truth for the heights of traffic signs, (h_t), 2) distances from the road boundary (d_t), and 3) tilt angles (α_t and α_p). For illustration, 10 of the 50 typical traffic signs were selected. The on-site measurement results are listed in the left section of Table III. Correspondingly, using the collected point cloud data of these traffic signs, the above parameters were also calculated by our proposed algorithm, details of the results are shown in the right section of Table IV.

In Table IV, negative values for d_t indicate that the boards of these traffic signs hang above the road surface and inside the curbs. Through statistics and analysis, the proposed algorithm achieved an accuracy of ± 0.063 m, ± 0.076 m, $\pm 52''$, and $\pm 37''$ for calculating h_t, d_t, α_t, and α_p, respectively, on these 10 traffic signs. On a whole, the proposed algorithm attained an accuracy of ± 0.07, ± 0.08, $\pm 54''$, and $\pm 42''$ for calculating h_t, d_t, α_t, and α_p, respectively, on the 50 selected traffic signs. Therefore, toward an accurate evaluation of the abnormalities and usability of traffic signs, our proposed algorithm is very promising and highly accurate for measuring traffic sign parameters. Similarly, no control point is used in the test, and the accuracy of the placement parameters measured will be further improved when control points are considered during the data acquisition.

VIII. CONCLUSION

This paper presented a spatial-related traffic sign inspection process for traffic sign inventory and management based on MLS data collected by a commercial MLS system, RIEGL VMX-450. The work demonstrated the potential for automated inspection of traffic sign boards and determination of spatial relations between traffic signs and the road environment using the 3-D MLS point clouds. Based on the high retro-reflective properties of traffic sign boards in MLS data, the proposed method works quite well in automated extraction of traffic sign boards from the laser scanned urban road scenes. From the surface points of the detected traffic sign boards, the developed registration algorithm projects those traffic sign board points onto a 2-D image plane for further image-based traffic sign recognition. Based on the detected traffic sign area in a 2-D image, a sign type recognition was conducted.

With the geo-spatial data acquired for the traffic sign and the connected road, inventory measurements were carried out. Taking the position and placement inspection as examples, our algorithm achieved several accurate inventory measurements, such as position, pose measurements, traffic sign planarity, etc. The experimental results demonstrated that the algorithms achieved detection precision of 91.63% and 92.61% on MLS point clouds and images, respectively; achieved precision of 96.32% for traffic sign type recognition. Moreover, with the achievement of sign type, position, and placement data, a spatial-associated sign network was built for a certain sign type and can be used for further ITS applications.

REFERENCES

[1] Manual on Uniform Traffic Control Devices for Streets and Highways, U.S. Dept. Transp. Federal Highway Admin., Washington, DC, USA, 2009 Edition.

[2] *Fixed, Vertical Road Traffic Signs—Part 1: Fixed Signs*, EN 12899-1:2007, May 2008.

[3] "Maintenance of signs and sign supports: A guide for local highway and street maintenance personnel," U.S. Dept. Transp. Federal Highway Admin., Washington, DC, USA, Jan. 2010.

[4] S. Maldonado-Bascon, S. Lafuente-Arroyo, P. Siegmann, H. Gomez-Moreno, and F. J. Acevedo-Rodriguez, "Traffic sign recognition system for inventory purposes," in *Proc. IEEE Intell. Veh. Symp.*, 2008, pp. 590–595.

[5] L. Hazelhoff, I. M. Creusen, and P. H. N. de With, "Robust detection, classification and positioning of traffic signs from street-level panoramic images for inventory purposes," in *Proc. IEEE WACV*, 2012, pp. 313–320.

[6] H. Gómez-Moreno, S. Maldonado-Bascón, P. Gil-Jiménez, and S. Lafuente-Arroyo, "Goal evaluation of segmentation algorithms for traffic sign recognition," *IEEE Trans. Intell. Transp. Syst.*, vol. 11, no. 4, pp. 917–930, Dec. 2010.

[7] Á. Gonzalez *et al.*, "Automatic traffic signs and panels inspection system using computer vision," *IEEE Trans. Intell. Transp. Syst.*, vol. 12, no. 2, pp. 485–499, Jun. 2011.

[8] H. Fleyeh and E. Davami, "Eigen-based traffic sign recognition," *IET Intell. Transp. Syst.*, vol. 5, no. 3, pp. 190–196, Sep. 2011.

[9] K. Lu, Z. Ding, and S. Ge, "Sparse-representation-based graph embedding for traffic sign recognition," *IEEE Trans. Intell. Transp. Syst.*, vol. 13, no. 4, pp. 1515–1524, Dec. 2012.

[10] F. Zaklouta and B. Stanciulescu, "Real-time traffic-sign recognition using tree classifiers," *IEEE Trans. Intell. Transp. Syst.*, vol. 13, no. 4, pp. 1507–1514, Dec. 2012.

[11] Á. González, L. M. Bergasa, and J. J. Yebes, "Text detection and recognition on traffic panels from street-level imagery using visual appearance," *IEEE Trans. Intell. Transp. Syst.*, vol. 15, no. 1, pp. 228–238, Feb. 2014.

[12] V. Tao and J. Li, *Advances in Mobile Mapping Technology*. London, U.K.: Taylor & Francis, 2007.

[13] J. Stallkamp, M. Schlipsing, J. Salmen, and C. Igel, "The German traffic sign recognition benchmark: A multi-class classification competition," in *Proc. Int. Joint Conf. Neural Netw.*, 2011, pp. 1453–1460.

[14] A. Møgelmose, M. M. Trivedi, and T. B. Moeslund, "Vision based traffic sign detection and analysis for intelligent driver assistance systems: Perspectives and survey," *IEEE Trans. Intell. Transp. Syst.*, vol. 13, no. 4, pp. 1484–1497, Dec. 2012.

[15] S. Šegvić, K. Brkić, Z. Kalafatić, and A. Pinz, "Exploiting temporal and spatial constraints in traffic sign detection from a moving vehicle," *Mach. Vis. Appl.*, vol. 25, no. 3, pp. 649–665, Apr. 2011.

[16] M. S. Prieto and A. R. Allen, "Using self-organizing maps in the detection and recognition of road signs," *Image Vis. Comput.*, vol. 27, no. 6, pp. 673–683, May 2009.

[17] S. Maldonado Bascón, J. Acevedo Rodríguez, S. Lafuente Arroyo, A. Fernández Caballero, and F. López-Ferreras, "An optimization on pictogram identification for the road-sign recognition task using SVMs," *Comput. Vis. Image Understand.*, vol. 114, no. 3, pp. 373–383, Mar. 2010.

[18] X. W. Gao, L. Podladchikova, D. Shaposhnikov, K. Hong, and N. Shevtsova, "Recognition of traffic signs based on their color and shape features extracted using human vision models," *J. Vis. Commun. Image Represent.*, vol. 17, no. 4, pp. 675–685, Aug. 2006.

[19] S. Salti, A. Petrelli, F. Tombari, N. Fioraio, and L. D. Stefano, "Traffic sign detection via interest region extraction," *Pattern Recognit.*, vol. 48, no. 4, pp. 1039–1049, Apr. 2015.

[20] J. Greenhalgh and M. Mirmehdi, "Real-time detection and recognition of road traffic signs," *IEEE Trans. Intell. Transp. Syst.*, vol. 13, no. 4, pp. 1498–1506, Dec. 2012.

[21] S. Houben, "A single target voting scheme for traffic sign detection," in *Proc. IEEE Intell. Veh. Symp.*, Jun. 2011, pp. 124–129.

[22] H. González-Jorge, B. Riveiro, J. Armesto, and P. Arias, "Geometric evaluation of road signs using radiometric information from laser scanning data," in *Proc. 2th Int. Conf. ISARC*, 2011, pp. 1007–1012.

[23] A. Ihara, H. Fujiyoshi, M. Takaki, H. Kumon, and Y. Tamatsu, "Improvement in the accuracy of matching by different feature subspaces in traffic sign recognition," *IEEJ Trans. Electron. Inf. Syst.*, vol. 129, no. 5, pp. 893–900, 2009.

[24] M. Takaki and H. Fujiyoshi, "Traffic sign recognition using SIFT features," *IEEJ Trans. Electron. Inf. Syst.*, vol. 129, no. 5, pp. 824–831, 2009.

[25] A. Ruta, Y. Li, and X. Liu, "Real-time traffic sign recognition from video by class-specific discriminative features," *Pattern Recognit.*, vol. 43, no. 1, pp. 416–430, Jan. 2010.

[26] A. Ruta, Y. Li, and X. Liu, "Robust class similarity measure for traffic sign recognition," *IEEE Trans. Intell. Transp. Syst.*, vol. 11, no. 4, pp. 846–855, Dec. 2010.

[27] X. Yuan, X. Hao, H. Chen, and X. Wei, "Robust traffic sign recognition based on color global and local oriented edge magnitude patterns," *IEEE Trans. Intell. Transp. Syst.*, vol. 15, no. 4, pp. 1466–1477, Aug. 2014.

[28] F. Zaklouta, B. Stanciulescu, and O. Hamdoun, "Traffic sign classification using k-d trees and random forests," in *Proc. Int. Conf. Neural Netw.*, 2011, pp. 2151–2155.

[29] D. Cireşan, U. Meier, J. Masci, and J. Schmidhuber, "Multi-column deep neural network for traffic sign classification," *Neural Netw.*, vol. 32, pp. 333–338, Aug. 2012.

[30] J. Stallkamp, M. Schlipsing, J. Salmen, and C. Igel, "Man vs. computer: Benchmarking machine learning algorithms for traffic sign recognition," *Neural Netw.*, vol. 32, pp. 323–332, Aug. 2012.

[31] J. Stallkamp, M. Schlipsing, J. Salmen, and C. Igel, "Introduction to the special issue on machine learning for traffic sign recognition," *IEEE Trans. Intell. Transp. Syst.*, vol. 13, no. 4, pp. 1481–1483, Dec. 2012.

[32] R. Timofte, K. Zimmermann, and L. V. Gool, "Multi-view traffic sign detection, recognition, and 3D localization," *Mach. Vis. Appl.*, vol. 25, no. 3, pp. 633–647, Apr. 2014.

[33] Z. Hu, "Intelligent road sign inventory (IRSI) with image recognition and attribute computation from video log," *Comput.-Aided Civil Infrastruct.*, vol. 28, no. 2, pp. 130–145, Feb. 2013.

[34] A. Habib, R. Uebbing, and K. Novak, "Automatic extraction of road signs from terrestrial color imagery," *Photogramm. Eng. Remote Sensing*, vol. 65, no. 5, pp. 597–601, 1999.

[35] D. Manandhar and R. Shibasaki, "Vehicle-borne Laser Mapping System (VLMS) for 3-D GIS," in *Proc. IEEE IGARSS*, 2001, vol. 5, pp. 2073–2075.

[36] Road Talk " A new tool for engineering surveys Mobile Terrestrial LiDAR Scanning (MTLS)," Ontario's Transp. Technol. Transfer Dig., Ministry Transp., Toronto, ON, USA, Spring 2013.

[37] L. Zhou and G. Vosselman, "Mapping curbstones in airborne and mobile laser scanning data," *Int. J. Appl. Earth Observ. Geoinf.*, vol. 18, pp. 293–304, Aug. 2012.

[38] B. Yang, L. Fang, Q. Li, and J. Li, "Automated extraction of road markings from mobile lidar point clouds," *Photogramm. Eng. Remote Sens.*, vol. 78, no. 4, pp. 331–338, 2012.

[39] S. Pu, M. Rutzinger, G. Vosselman, and S. O. Elberink, "Recognizing basic structure from mobile laser scanning data for road inventory studies," *ISPRS J. Photogram. Remote Sens.*, vol. 66, no. 6, pp. s28–s39, Dec. 2011.

[40] H. Guan, J. Li, Y. Tao, M. Chapman, and C. Wang, "Automated road information extraction from mobile laser scanning data," *IEEE Trans. Intell. Transp. Syst.*, vol. 16, no. 1, pp. 194–205, Feb. 2015.

[41] B. Yang and Z. Dong, "A shape-based segmentation method for mobile laser scanning point clouds," *ISPRS J. Photogramm. Remote Sens.*, vol. 81, pp. 19–30, Jul. 2013.

[42] Z. Zhang, "A flexible new technique for camera calibration," Microsoft Res., Redmond, WA, USA, Tech. Rep. MSR-TR-98-71, Dec. 1998.

[43] J. Weijer and C. Schmid, "Coloring local feature extraction," in *Proc. ECCV*, 2006, pp. 334–348.

[44] N. Dalal and B. Triggs, "Histograms of oriented gradients for human detection," in *Proc. IEEE CVPR*, 2005, pp. 886–893.

[45] Y. Yu, J. Li, H. Guan, and C. Wang, "Automated extraction of urban road facilities using mobile laser scanning data," *IEEE Trans. Intell. Transp. Syst.*, DOI: 10.1109/TITS.2015.2399492. [Online]. Available: http://ieeexplore.ieee.org/xpl/articleDetails.jsp?tp=&arnumber=7047870&queryText%3D10.1109%2FTITS.2015.2399492

[46] L. Breiman, "Random forests," *Mach. Learn.*, vol. 45, no. 1, pp. 5–32, 2002.

Chenglu Wen (M'14) received the Ph.D. degree in mechanical engineering from China Agricultural University, Beijing, China, in 2009. She is currently an Assistant Professor with Fujian Key Laboratory of Sensing and Computing for Smart City, School of Information Science and Engineering, Xiamen University, Xiamen, China. She has coauthored more than 30 research papers published in refereed journals and proceedings. Her current research interests include machine vision, machine learning, and point cloud data processing. She is the Secretary of the ISPRS WG I/3 on Multi-Platform Multi-Sensor System Calibration (2012–2016).

Jonathan Li (M'00–SM'11) received the Ph.D. degree in geomatics engineering from the University of Cape Town, Cape Town, South Africa. He is currently a Professor with the MoE Key Laboratory of Underwater Acoustic Communication and Marine Information Technology, School of Information Science and Engineering, Xiamen University, Xiamen, China. He is also a Professor with and the Head of the GeoSTARS Laboratory, Faculty of Environment, University of Waterloo, Waterloo, ON, Canada. He has coauthored more than 300 publications, over 100 of which were published in refereed journals including IEEE-TGRS, IEEE-TITS, IEEE-GRSL, ISPRS-JPRS, IJRS, PE&RS, and RSE. His current research interests include information extraction from mobile LiDAR point clouds and from earth observation images. He is the Chair of the ISPRS WG I/Va on Mobile Scanning and Imaging Systems (2012–2016), the Vice Chair of the ICA Commission on Mapping from Remote Sensor Imagery (2011–2015), and the Vice Chair of the FIG Commission on Hydrography (2015–2018).

Huan Luo received the B.Sc. degree in computer science from Nanchang University, Nanchang, China, in 2009. He is currently working toward the Ph.D. degree with Fujian Key Laboratory of Sensing and Computing for Smart City, School of Information Science and Engineering, Xiamen University, Xiamen, China. His current research interests include computer vision, machine learning, and mobile LiDAR point cloud data processing.

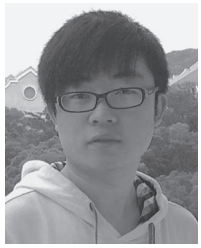

Yongtao Yu received the B.Sc. degree in computer science from Xiamen University, Xiamen, China, in 2010. He is currently working toward the Ph.D. degree with Fujian Key Laboratory of Sensing and Computing for Smart City, School of Information Science and Engineering, Xiamen University. His current research interests include computer vision, machine learning, and LiDAR point cloud processing.

Zhipeng Cai received the B.Sc. degree in computer science from Xiamen University, Xiamen, China, in 2013. He is currently working toward the M.Sc. degree with Fujian Key Laboratory of Sensing and Computing for Smart City, School of Information Science and Engineering, Xiamen University. His current research interests include computer vision, machine learning, and LiDAR point cloud processing.

Hanyun Wang (M'13) received the M.Sc. degree in information and communication engineering in 2010 from the National University of Defense Technology, Changsha, China, where he is currently working toward the Ph.D. degree with the School of Electronic Science and Engineering. His research interests include computer vision, machine learning, and LiDAR point cloud processing.

Cheng Wang (M'11) received the Ph.D. degree in information and communication engineering from the National University of Defense Technology, Changsha, China, in 2002.

He is currently a Professor with and the Associate Dean of the School of Information Science and Engineering and the Executive Director of Fujian Key Laboratory of Sensing and Computing for Smart City, both at Xiamen University, Xiamen, China. He has coauthored more than 80 papers in referred journals, including IEEE-TGRS, IEEE-TITS, IEEE-GRSL, IEEE-JSTARS, IJRS, and ISPRS-JPRS. His current research interests include remote sensing image processing, mobile LiDAR data analysis, and multisensor fusion. He is a Cochair of the ISPRS WG I/3 on Multi-Platform Multi-Sensor System Calibration (2012–2016) and a Council Member of China Society of Image and Graphics.